Postprint of: Faizan M., Wang X., Abdelmohsen S. A. M., Bhamu K. C., Sappati S., Laref A., Muhammad N., Mushtaq M., Abdelbacki A. M. M., Khenata R., Understanding the Electronic Structure and Optical Properties of Vacancy-Ordered Double Perovskite A_2BX_6 for Optoelectronic Applications, ENERGY & FUELS, (2022), DOI: 10.1021/acs.energyfuels.2c00341

Understanding the electronic structure and optical properties of vacancy ordered double perovskite A_2BX_6 for optoelectronic applications

Muhammad Faizan[a*], Xinjiang Wang[b*], Shaimaa A. M. Abdelmohsen[c], K. C. Bhamu[d], Subrahmanyam Sappati[e,f], Amel Laref[g], Nisar Muhammad[h], Muhammad Mushtaq[i], Ashraf M. M. Abdelbacki[j], Rabah Khenata[k]

[a]Department of Physics, University of Peshawar, Peshawar 25120, Pakistan
[b]State Key Laboratory of Superhard Materials, College of Physics, Jilin University, Changchun 130012, China
[c]Department of Physics, College of Science, Princess Nourah bint Abdulrahman University, P.O. Box 84428, Riyadh 11671, Saudi Arabia
[d]School of Chemical Engineering, University of Ulsan, 93 Daehakro, Nam-Gu, Ulsan 44610, South Korea
[e]Department of Pharmaceutical Technology and Biochemistry, Gdańsk University of Technology, Narutowicza 11/12, 80-233 Gdańsk, Poland
[f]BioTechMed Center, Gdańsk University of Technology, Narutowicza 11/12, 80-233 Gdańsk, Poland
[g]Department of Physics and Astronomy, College of Science, King Saud University, Riyadh, 11451, Saudi Arabia
[h]Hefei National Research Center for Physical Sciences at the Microscale and Department of Physics, University of Science and Technology of China, Hefei, Anhui 230026, P.R. China
[i]Department of Physics, University of Poonch Rawalakot, 12350, Pakistan
[j]Deanship of Skill development, King Saud University, Riyadh 11451, Saudi Arabia
[k]Laboratoire de Physique Quantique et de la Matière et de Modélisation Mathématique (LPQ3M), Université de Mascara, 29000 Mascara, Algeria
*Correspondence: faizanstd@uop.edu.pk, xjwang.jlu@gmail.com

Abstract

Over the past few years, metal halide perovskite solar cells have made significant advances. Currently, the single-junction perovskite solar cells reach a conversion efficiency of 25.7%. Perovskite solar cells with wide band gap can also be used as top absorber layers in multi-junction tandem solar cells. We examined the dynamical and thermal stability, electronic structure, and optical features of In_2PtX_6 (X=Cl, Br, I), utilizing first-principle calculations. The stability is predicted using phonon dispersion spectrum, AIMD simulation, and also through the convex hull approach. The lattice constants and the optimized volume show an increasing trend with changing halide ions. The band structures computed for In_2PtCl_6, In_2PtBr_6, and In_2PtI_6 indicate semiconducting nature with band gap values of 2.06, 2.01, and 1.35 eV, respectively. Halogens *p* and Pt-*d* orbitals, respectively, play a prominent role in the formation of states around VBM and CBM. The compounds, namely In_2PtBr_6 and In_2PtI_6, exhibit high dielectric constants and small carrier effective masses. Furthermore, we found that

In_2PtI_6 reveals a maximum theoretical efficiency owing to its optimum band gap and high optical absorption, and is comparable to $MAPbI_3$ in the studied range. Our results suggest that In_2PtX_6 (X=Cl, Br, I) are suitable materials for single-junction and top absorber layers in tandem solar cells.

Keywords: Perovskites Solar cells; electronic structure; First-principles; halide perovskites; Optical absorption, band structure

1. Introduction

Solar energy is directly converted into electrical energy by utilizing photovoltaic effects in solar cells. Among the advantages of solar cells are being renewable, clean, safe, environmentally friendly, and long-lived. In terms of renewable energy sources, they are one of the most prospective technologies. The emergence of halide perovskites-based solar cells has completely changed the field of solar cells because of their rapidly increasing efficiency and controllability in material growth and structure.[1-2] For feasible utilization in third-generation photovoltaic devices, halide perovskites, particularly hybrid organic-inorganic or pure inorganic halides, such as ammonium iodide $CH_3NH_3PbI_3$, $CsSnI_3$, and others, have been extensively explored.[3-6] As a result of their superior optoelectronic characteristics and high photoelectric conversion efficiency,[7-9] they have gained considerable research attention from the scientific community and have progressed quickly over the last few years. In only a decade, the organic-inorganic hybrid perovskites compound has achieved a light conversion efficiency of 25.7% (2022) from an original value of 3.81% (2009).[10-11] However, perovskites solar cells have a few major bottlenecks in the commercial application, involving the instability of lead-based perovskite solar cells and the degradation of the absorber layer when exposed to water or heat, as well as the toxicity of the heavy metal lead.[2, 12-15] Therefore, seeking new perovskites solar cell materials that are non-toxic, environmental friendliness, and high in conversion efficiency has turned into one of the hottest topics in solar cell research.

Halide perovskites have a general stoichiometry in the form of ABX_3, where 'X' refers to a monovalent halogen anion, 'A' denotes a monovalent (organic/inorganic) cation, and 'B' represents a divalent transition metal cation. Various alternatives of perovskite materials have been developed depending on the compositional and structural diversity of perovskite compounds. The vacancy-ordered double perovskites A_2BX_6 can be derived from a cubic halide perovskite (ABX_3) by removing half of the B atoms at the center of the octahedron in a regular motif.[16] In order to preserve charge neutrality, B-atom must be in +4 oxidation state, which enables an extensive span of cations to be used at the octahedral B-site.[17] Initially, the

compound called Cs_2SnI_6 has been favourably applied as a hole transport material for all-solid-state dye-sensitized solar cells (DSSC) and has attained ~8% efficiency.[18] Likewise, $Cs_2TiI_2Br_4$ and Cs_2TiBr_6 are considered appropriate materials for single- and multi-junction perovskite solar cells due to their suitable band gap, enhanced environmental stability, and benign defect tolerance.[19-20] A maximum of 3.3% efficiency can be reached for these promising compounds. In a recent report, Cs_2PtI_6 perovskite was found to achieve a higher power-conversion-efficiency of 13.88%.[21] Researchers are seeking different variants to further enhance the power conversion efficiency of A_2BX_6 perovskites.

Recent studies on vacancy-ordered double perovskite A_2BX_6 (A= alkali metals; B= Sn, Te, or transition metals; and X= halides) have been reported, providing new prospects for a stabilized and environmentally-friendly solar cell material.[22-23] In particular, Rb_2PdI_6, Rb_2PdBr_6, and Cs_2PtI_6 compounds exhibit an optimum band gap, large dielectric constant, and high absorption coefficient, which offer advantages to a stable and eco-friendly material for solar cells technology. Similarly, the pure inorganic compounds Cs_2SnCl_6, Cs_2SnBr_6, and Cs_2SnI_6 exhibit stable crystal structures at ambient temperature, possess direct band gap semiconducting character, and are found suitable for dye-sensitized solar cells.[24] In particular, the dye-sensitized solar cell based on Cs_2SnI_6 has a photoelectric conversion efficiency of 4.23%, and there is still much room for improvement in the future. Zhao et al. employed DFT-based first-principles calculations to investigate the electronic structure and optical features of inorganic A_2PtI_6 (A= Rb or Cs) compounds.[25] In addition to their optimum band gap values of 1.15 eV and 1.29 eV, these compounds exhibit excellent light absorption, making them suitable for photovoltaic applications. Another study has examined the electronic and transport characteristics of Cs_2PtI_6 for its potential applications as a favourable thermoelectric material.[26] At 300 K, the compound possesses ultralow thermal conductivity (0.15 W/mK), a remarkable Seebeck coefficient (139 μV/K), and a high figure of merit (1.03). Very recently, Alhodaib explored the optoelectronic and thermoelectric properties of In_2PtX_6 (X = Cl, Br, I) using PBE and mBJ parameterization schemes.[27] The geometric structure, electronic band gap, and thermoelectric transport coefficient for improved solar cell and thermoelectric application was investigated. The author reported band gap in the range of 1.30 to 2 eV and figure of merit (0.8 to 1) at T= 300 K.

Based on the above literature, we concluded that the Pt-containing compounds are preferred for potential applications in solar energy and other optoelectronic technologies. Using theoretical approach based on DFT, this paper describes the stability, crystal geometry, electronic structure, and optical characteristics of In_2PtCl_6, In_2PtBr_6, and In_2PtI_6 compounds.

Our findings shed light on the fundamental features that pertain closely to their application in solar cells and are difficult to measure experimentally, such as thermodynamic and thermal stability, electronic band gap, optical absorption coefficient, the density of states, and dynamical dielectric function. We also summarize our findings regarding the effective mass and spectroscopic limited maximum efficiency. The compounds possess energy band gaps between 1.35 to 2.06 eV and a pronounced absorption coefficient, making them suitable for single- and multi-junction photovoltaic devices. Hopefully, our investigation will serve as theoretical guidance to future research on vacancy ordered perovskites for photovoltaic and other energy applications.

2. Computational Methods

First-principles calculations are conducted utilizing the full-potential all-electron method (FP-LAPW), integrated with the wien2k simulation package.[28] A solid's structural, electronic, and optical characteristics can be accurately predicted by employing this method.[29] Based on a generalized gradient approximation (GGA), the exchange-correlation functional is implemented in terms of the Perdew–Burke–Ernzerhof (PBE)[30] and modified Becke Johnson (mBJ) potential.[31] We also tested the hybrid functional through Heyd–Scuseria–Ernzerhof (HSE) scheme for band gap comparison.[32] In addition, the spin-orbit coupling (SOC) effect was also computed, resulting in a significant reduction in the band gap. In the first step, the atomic structure of In_2PtCl_6, In_2PtBr_6, and In_2PtI_6 were relaxed and optimized using the PBE functional. After that, we employ the mBJ potential on top of PBE-GGA relaxed lattice parameters for calculating the electronic structure and other physical properties of these systems.

Calculations were carried out using the charged density expansion up to the reciprocal vector G_{max}=12 $a.u^{-1,}$ and the radial wave function (l_{max}) was expanded to its maximum value up to 12. The atomic position within the considered structure was fully relaxed until the electronic charge, and atomic force on each atom converged and attain values of 0.0001 $|e|$ and 10^{-5} Ry/Bohr, whereas the total energy for self-consistent field calculation was converged to 0.001 Ry. A 1000 k-points mesh has been employed to integrate the first Brillouin zone (BZ) with the RK_{max}= 8 (the radius R denotes the smallest muffin tin sphere in the unit cell, and K_{max} represents the maximum k-vector) for self-consistent field calculations. A cutoff of -7.0 Ry is used to separate the core region from the valence states region. We adopted a denser mesh with 5000 k-points in the irreducible Brillouin zone to ensure convergence for electronic

and optical characteristics of the studied materials. Further detail about the optical computation, phonon calculations, and *ab-initio* moleculer dynamic simulations can be found in Supplementary information.

3. Results and Discussion

3.1 Structural features of In_2PtX_6

After relaxation, the In_2PtX_6 (X=Cl, Br, I) compounds exhibit a cubic crystal structure (archetype K_2PtCl_6) with standard face-centered cubic space group $Fm\bar{3}m$. The crystal structure of In_2PtX_6 is depicted in Figure 1. The vinaceous, yellow-orange, and bluish spheres portray In, Pt, and X atoms. In this structure, the Pt and X atoms are bonded octahedrally $[PtX_6]^{2-}$, with the In^+ cations embedded between these octahedrons to form a cuboctahedral environment. Each In^+ atom forms an In-Pt bond with a coordination number of 12. In In_2PtX_6, each Pt atom is surrounded by 6 nearest neighbor X atoms, forming $[PtX_6]$ octahedral units. The cubic phase of In_2PtX_6 shares many similarities with the typical ABX_3 perovskite in structure and can be viewed as the result of vacancy defects forming in ABX_3 perovskite.[24, 33]

Cell Parameters

The PBE optimized energy versus volume data was computed using the Birch Murnaghan's equation and is illustrated in Figure 2. The lattice constants of In_2PtX_6 acquired after geometry optimization using different GGA schemes are presented in Table 1. From the listed data, it can be noticed that the lattice constants of In_2PtX_6 increase as the atomic number of the halogen anion increases, which is primarily attributed to the increasing radius of the halogen anion at the X position. The lattice constant of In_2PtX_6 cannot be compared since the experimental data is unavailable. However, our calculation show consistency with recently published data based on PBE functional.[27] In Table 2, the bond lengths of Pt-based perovskites are collected. Based on our findings, the bond lengths In-X (X= Cl, Br, I) and Pt-X indicate an increasing tendency with the halogen size Cl (1.84) < Br (1.96) < I (2.20). In particular, the iodide-comprising perovskite such as In_2PtI_6 exhibits a larger lattice constant due to a longer bond length. Furthermore, replacing anions with different electronegativity can modify the electronic structure and reduce the dependence of the material characteristics on the crystal structure dimension.

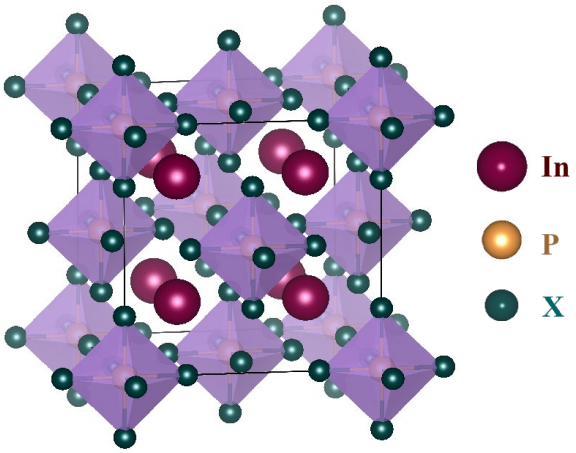

Figure 1. Schematic illustration of the In_2PtX_6 crystal structure.

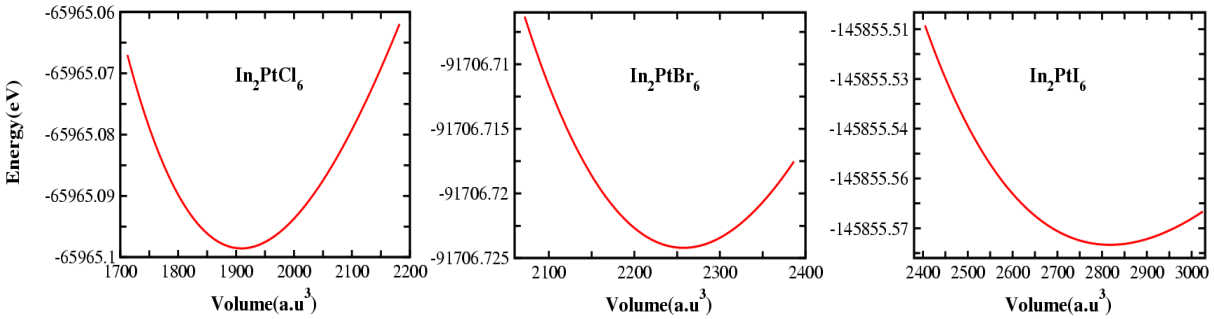

Figure 2. The calculated total energy versus volume curves for inorganic In_2PtX_6 halide perovskites.

Table 1. The optimized lattice parameters of In_2PtCl_6, In_2PtBr_6, and In_2PtI_6, obtained using different GGA functional.

Compound	Lattice constants (Å)				Volume (Å^3)	Bulk Modulus (GPa)	Energy(Ry)
	PBE	WC	PBEsol	Other works			
In_2PtCl_6	10.18	10.007	9.99	10.42[27]	1010.24	36.24	-65965.09
In_2PtBr_6	11.01	10.80	10.79	11.02[27]	1194.63	29.43	-91706.72
In_2PtI_6	11.82	11.61	11.59	11.86[27]	1491.18	22.59	145855.58

Table 2. The calculated bond length for In_2PtCl_6, In_2PtBr_6, and In_2PtI_6 perovskites.

In–Pt	In–Cl/Br/I	Pt–Cl/Br/I
4.33	3.54	2.34
4.53	3.70	2.49
4.84	3.95	2.69

Stability

To assess the dynamical and thermal stability of A_2BX_6 based halide perovskites (A = In; B = Pt; and X = Cl, Br, and I), we performed self-consistent phonon calculation and *ab initio* molecular dynamics (MD) simulation.

From the phonon dispersion spectrum (Figure 3), it can be found that at T= 0 K, there are soft modes with negative frequencies (at gamma and other symmetry points of the BZ) for all the understudy compounds, which shows that the In_2PtX_6 perovskites are dynamically unstable. The major cause of the soft phonon modes in the In_2PtX_6 structure is the two-fold rattling of In and PtX_6 octahedral cluster.[34] However, at T= 300K, no imaginary frequencies appear in the whole BZ, demonstrating the dynamical stability of In_2PtX_6 at high temperatures. Our results are consistent with a recently published work and suggest that the studied compounds are likely to be synthesized in experiments.

Further, the thermal stability is confirmed by conducting the *ab initio* molecular dynamics (MD) simulation using the canonical NVT ensemble with a Nosé thermostat model.[35] We performed the AIMD simulations at 300 K up to 5 ps to verify its thermodynamic stability and plotted the results in Figure 4. The MD simulations at 300 K confirmed the thermal stability of In_2PtX_6, revealing that free energy fluctuates within a limited energy span after a time of 5 ps (Figure 4). As a result, the proposed compounds can be synthesized under appropriate experimental conditions. In addition, the well-known convex hull method was also employed to investigate the thermodynamic stability of the compounds (see Supplementary Information for detail). Table S1 contains the complete list of competing phases as well as the calculated formation energies. The chemical potential ranges of the compounds as well as their possible binary and ternary phases, are given in a 2D plane in Figure S1. It is seen that all of the compounds have positive formation energy, which implies their unstable nature. As a result, our findings indicate that synthesizing the In_2PtX_6 perovskite under thermal equilibrium growth conditions may be difficult, and specific experimental conditions, such as high pressure and high temperature, must be regulated in order to synthesize the In_2PtX_6 perovskites.

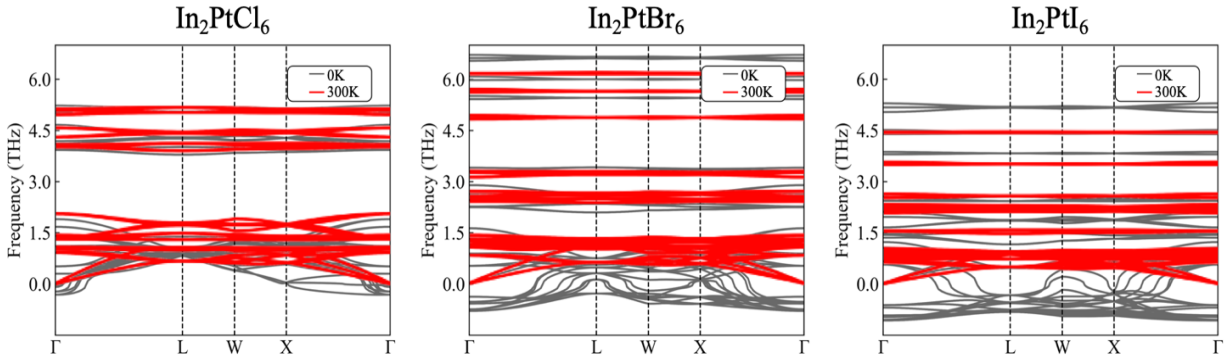

Figure 3. Calculated phonon spectrum of In_2PtCl_6, In_2PtBr_6, and In_2PtI_6 at 0 and 300 K.

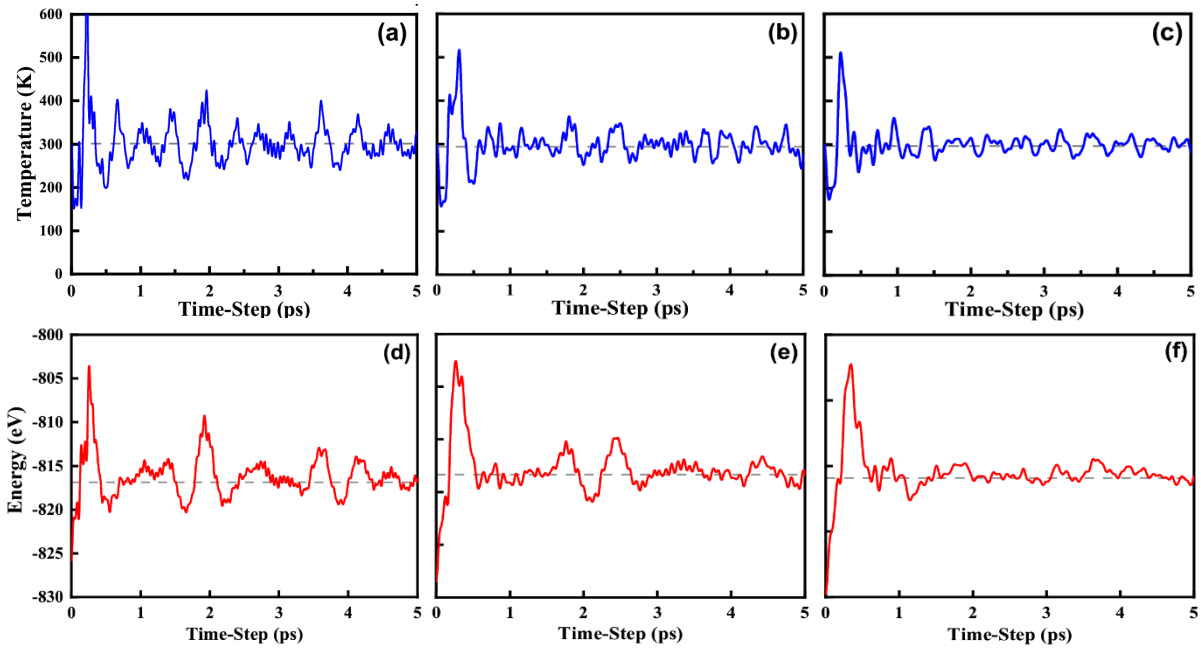

Figure 4: The AIMD simulation of In_2PtCl_6, In_2PtBr_6, and In_2PtI_6 perovskite at 5 ps with temperature-controlled at 300 K using NVT ensemble. The upper panel (a-c) shows temperature evolution with time, while the lower panel (d-f) shows variation of energy with time at 300 K.

3.2 Electronic Properties

After discussing the crystal structure and stability of these systems, we investigated their-band structures utilizing PBE, mBJ, and HSE functional. Table 3 summarizes the calculated band gap values of In_2PtCl_6 (2.06 eV), In_2PtBr_6 (2.01 eV), and In_2PtI_6, (1.35 eV) from mBJ potential as well as other schemes. Among In_2PtX_6 (X= Cl, Br, I), In_2PtCl_6 possesses direct band gap character, while In_2PtBr_6 and In_2PtI_6 exhibit an indirect band gap semiconducting property (Figure 5). However, the direct band gap values are somewhat larger than the indirect gap by a few meV. The quasi-direct band gap character of In_2PtX_6 is fairly similar to that of Cs_2TiI_6[19] and Cs_2PdBr_6.[36] Likewise, the band gap of the three systems reveals a decreasing trend with the halogen atomic number. In the three energy band structures, the valence band maximum is artificially aligned to 0 eV, while the conduction band positions continue to move toward lower energy levels with changing halide ions. As we move down the group from Cl to I, the band gap decreases from 2.06 eV in In_2PtCl_6 to 1.35 eV in In_2PtI_6 due to the raising of halogen *p*-orbitals (in energy) relative to the indium states. This is analogous to the trend seen in Pb based perovskites $CH_3NH_3PbX_3$ (X= Cl, Br, I).[37] Additionally, it is worth noting that the dispersion

of the conduction band likely comes from the dispersive halide *p* states, and its band width decreases by changing the halide ions consecutively from Cl to Br and Br to I. In accordance with the well-known Shockley-Queisser limit theory[38], ideal single p-n junction solar cells possess the optimal theoretical photoelectric conversion efficiency (~33%) with a 1.34 eV band gap of the absorber layer. The theoretical band gap value of In_2PtI_6 is 1.35 eV, which is akin to the ideal band gap value for a single junction photovoltaic cell. The remaining two compounds, In_2PtCl_6 and In_2PtBr_6, with band gap values of 2.06 eV and 2.01 eV, are suitable for use in the top cell in multi-junction tandem cells. In HSE06 calculations, In_2PtCl_6 and In_2PtBr_6 compounds show relatively larger band gap of 2.37 and 2.26 eV, whereas In_2PtI_6 shows a suitable band gap of 1.63 eV (Table 3). We have also tested the spin-orbit coupling (SOC) effect on the electronic properties of In_2PtX_6 perovskites. The SOC significantly reduces the band gap of In_2PtX_6 in both the PBE-SOC and mBJ-SOC schemes (Table 3 & Figure S2). Based on our observations, the band gap of In_2PtX_6 (X= Cl, Br, I) compounds have never been reported experimentally and were predicted for the first time in our work.

Figures 6 displays the computed total and partial electronic density of states (DOS) of halide perovskites In_2PtX_6. The uppermost valence bands are made of *p* orbitals of halogen (Cl/Br/I), dispersed in the energy range between 0 eV and −1.5 eV. The VBM comprises halogen 3*p* orbitals for In_2PtCl_6 and replaces the 3*p* orbital with the higher energy orbital (4*p*@ In_2PtBr_6 and 5*p*@ In_2PtI_6), reducing the band gap across In_2PtX_6 (X=Cl, Br, I). Additionally, we find that the In 5*s* and Pt 5*d* orbitals have a minor contribution to the VBM, indicating that the Pt-5*d* and X-*p* orbitals exhibit a weak anti-bonding interaction. The 5*d* orbitals of Pt are mostly distributed in the energy span of –5.7 to –4.9eV (In_2PtCl_6), –4.08 to –3.2eV (In_2PtBr_6), and –3.9 to –3.2 eV (In_2PtI_6), while their anti-bonding orbitals are located at the high energy of the conduction band. Moreover, the lowest conduction band of these systems is primarily made of Pt 5*d* and X-*p* orbitals. The higher conduction bands dispersed in the energy range from ~4.5 to ~6 eV (In_2PtCl_6 and In_2PtBr_6) and from ~3.4 to ~4.3 eV (In_2PtI_6) are dominated by In-5*p* orbitals.

Next, we consider the electron and hole effective mass by analysing the electronic band structure of In_2PtX_6 compounds. In order to calculate it, we take the second derivative of the energy, E (k), versus the wave vector k around the lowest conduction band minimum and valence band maximum, by $m^* = \hbar^2[\partial^2 E(k)/\partial^2 k]^{-1}$ (m^*: effective mass). According to the band dispersion, the effective masses for the In_2PtX_6 (X=Cl, Br, I) perovskites are determined in two directions. Table 4 shows the anisotropic electron/hole effective masses and the averages

of the effective masses along two different branches, which are labelled with bold values. We see from the band structure near the Fermi level (Figure S3) that while going from In_2PtCl_6 to In_2PtI_6, the top of the valence band is approaching band convergence[39]. It gives degenerate states at the Γ symmetry point, which results in the heavy hole (labelled as HH) and light hole (LH) components of the valence states in the case of In_2PtI_6. We calculated the effective mass for both heavy hole and light hole (Table 4). The electron effective masses span the range of 0.43 to 0.69 m_0, while the hole effective masses range from 0.60 to 15.27 m_0. For the light hole, the effective mass lies between 0.53 and 0.68, whereas the heavy hole mass is approaching 29.34m_0. In fact, the electron effective mass is relatively smaller than the hole effective mass, which is similar to the trend seen in Cs_2SnI_6 and other A_2BX_6 perovskites.[22, 40-41] The smaller effective mass from the light hole and band degeneracy contributes to the high mobility of carriers, thus enhancing the optical performance of In_2PtI_6[42] compared to the other two systems. For In_2PtCl_6 and In_2PtBr_6, we found a small band convergence (0.0017eV@In_2PtCl_6 and 0.0087eV@In_2PtBr_6) which is responsible for the moderate optoelectronic performance of these systems. Further, the electron effective mass of In_2PtBr_6 is found comparable to the lead-based $MAPbI_3$ (0.42m_0) perovskites.[43]

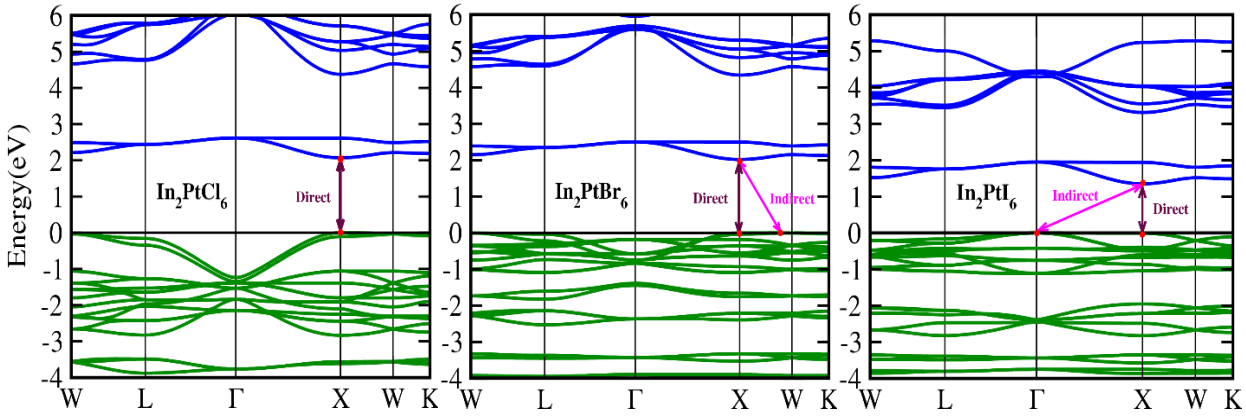

Figure 5. Band structure diagrams of In_2PtX_6 calculated by mBJ potential. The valence bands are shown in olive, and the VBM is positioned at 0 eV in each case, while the conduction bands are shown in blue.

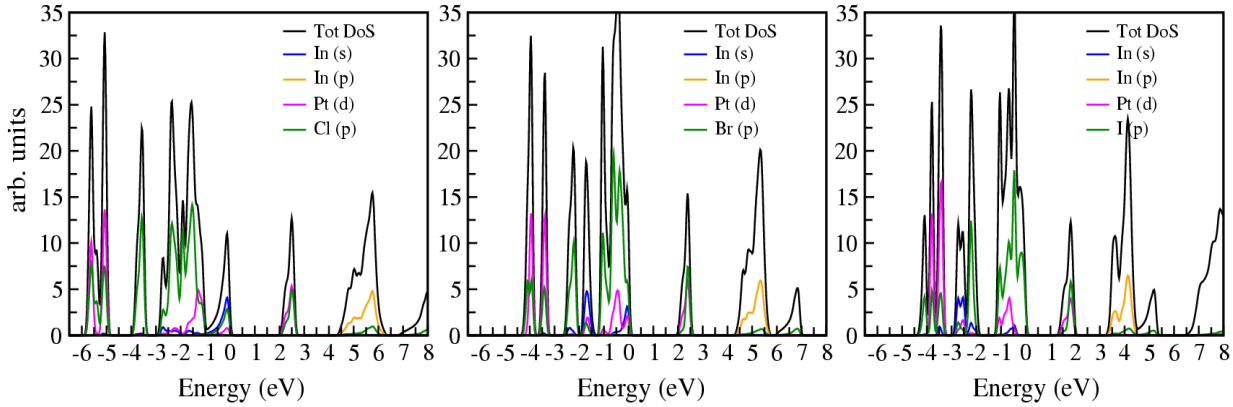

Figure 6. Computed partial and total density of states of In_2PtX_6 by mBJ method.

Table 3. The computed band gap values of In_2PtX_6 (X= Cl, Br, I) using different approximation.

Compound	PBE	PBE-SOC	mBJ	mBJ-SOC	HSE	Other works*
In_2PtCl_6	1.60	1.46	2.06	1.70	2.36	2.0
In_2PtBr_6	1.58	1.44	2.01	1.77	2.29	1.96
In_2PtI_6	0.81	0.73	1.35	1.30	1.63	1.30

*Ref. 27

Table 4. The electron and hole effective masses of In_2PtX_6 (X= Cl, Br, I) perovskites calculated in different directions. The calculated effective masses use the unit of free electron rest mass (m_0 = 9.11 x 10^{-31} kg).

Compounds	m_e		m_h			
In_2PtCl_6	0.62(X- Γ)	0.72(X-W)	2.40 (W-X)		6.78 (W-K)	
	0.67		**4.59**			
In_2PtBr_6	0.42(X- Γ)	0.45(X-W)	1.10 (W-X)		3.68 (W-K)	
	0.43		**2.39**			
In_2PtI_6	0.62(X- Γ)	0.76(X-W)	1.20 (Γ-W) (HH)	29.34 (Γ-X) (HH)	0.68 (Γ-W) (LH)	0.53 (Γ-X) (LH)
	0.69		**15.27**		**0.60**	

3.3 Optical Properties

It is crucial to determine the dielectric constant and absorption spectrum of a material in order to understand its optical properties. From the sum of all direct valence band transitions to the

conduction band, one can estimate the imaginary part of the dielectric constant (ε_2). The real part of the dielectric response (ε_1) can be estimated by solving the Kramers-Kronig relations. A high dielectric constant is regarded as a primary index for efficient photovoltaic absorbers because it assists electron-hole separation and screening charged defects.

The static dielectric constant consist of electronic $\varepsilon_\infty(\omega)$ and ionic $\varepsilon_{ion}(\omega)$ contribution. In this study, we consider both the electronic and ionic parts for In_2PtX_6 (X=Cl, Br, I) in different directions. The values of dielectric constants increase monotonically with changing halide ion (Cl→Br→I), as shown in Table S2 and Figure 7. Specifically, In_2PtI_6 displays large static dielectric constants, making it more significant than In_2PtCl_6 and In_2PtBr_6. A high static dielectric constant allows carriers to be screened from charged defects in a crystal, causing less carrier trapping and scattering. The scattering reduction can enable semiconductors to achieve longer carrier diffusion lengths and larger mobility lifetime outcomes. As photon energy increases, the spectra of all these compounds illustrate an increasing tendency. In the visible spectrum, both In_2PtI_6 and In_2PtBr_6 spectra display the first prominent peak at 1.72 and 1.88 eV, followed by multiple peaks at various photon energies. The compound, namely In_2PtI_6, exhibits a maximum dielectric constant of magnitude 11.70 at ~3.82 eV. For In_2PtCl_6 and In_2PtBr_6, the dielectric constant reaches the maximum peak values of 9.08 and 9.75, respectively, at ~4.03 eV. Further, one can see in Figure 7 that changing the halide from Cl to I in In_2PtX_6 redshifts the curves towards the visible energy span with increased amplitude. This leads to an increase in the ε_1 spectra, and the peaks shift to lower energies.

The imaginary part indicates the amount of absorption or dissipation of light while passing through a material. Figure 7 (left panel) presents the calculated imaginary dielectric spectra of In_2PtX_6. Dielectric spectra show different peaks with variable amplitudes caused by possible electronic transitions from the valence band to the conduction band. In the visible light span, the first spectral peak of $\varepsilon_2(\omega)$ curve consists of the optical transitions between the highest valence bands of X-p (Cl-3*p*, Br-4*p,* or I-5*p*) and the lowest conduction bands of Pt-5*d* states. It was found that the second-highest peak in the energy span of 3.8 to 5.7 eV was primarily caused by the optical transitions from the highest valence bands of Cl-3*p*, Br-4*p*, or I-5*p* orbitals to the conduction bands of In-6*s* orbitals (not displayed for brevity), which lie far from the Fermi level. For In_2PtI_6, In_2PtBr_6, and In_2PtCl_6, their maximum values of 12.74 occur at ~4.24 eV, 11.23 at 4.61 eV, and 10.70 at 5.01 eV, respectively. Compared to In_2PtBr_6 and In_2PtCl_6, the iodide containing compounds In_2PtI_6 exhibits a significant peak (6.62) at 2.20 eV, indicating its intense response to the visible light. In addition, this finding further demonstrates

the usefulness of inorganic In_2PtX_6 perovskites as a reliable replacement for organolead halide perovskites.

The absorption coefficient represents another important characteristic for photovoltaic characterization of semiconductors. It controls the penetration of light in a medium and offers a direct indicator of the ability of a semiconductor to harvest light. The computed absorption spectra of In_2PtX_6 in the photon energy region between 0 and 3.1 eV is displayed in Figure 8. For all compounds, the absorption spectra show prominent peaks in the visible as well as the ultraviolet spectral region (not shown for brevity). It can be noticed that their absorption coefficients exceed 10^5 cm^{-1}, and In_2PtI_6 and In_2PtBr_6 compounds have optimum light absorption characteristics in the visible light span, while In_2PtCl_6 exhibits optimum absorption properties in the ultraviolet region. In the visible spectrum, In_2PtI_6 displays a maximum light absorption of 2.17×10^5 cm^{-1} at a photon energy of 2.59 eV, while In_2PtBr_6 exhibits optimal absorption value of 2.20×10^5 cm^{-1} at ~2.87 eV. The maximum absorption coefficient in the visible spectrum mainly comes from the large and localized density of states near the lowest conduction band as well as their low band gap. In addition, as halogen anions become larger, the absorption spectrum moves to the redshift direction, consistent with the band gap trend discussed above. The solar absorber with high absorption coefficient is particularly desirable for cell performance as photogenerated carriers are not required to travel far before being recombined. Consequently, the non-radiative recombination is substantially reduced while simultaneously increasing the open circuit voltage of the photovoltaic cells.[44] Because of the high absorption coefficients, thin absorber layers can be used, reducing the fabrication costs of solar cells.[45]

In addition to these optical features, refractive index n(ω), extinction coefficient k(ω), reflectivity R(ω), and energy-loss function L(ω) are essential optical parameters for solar cells to perform well. The reflectivity of material is represented by the ratio of the reflected light energy from its surface to the amount of incident light energy. It is regarded as an essential optical property for photovoltaic applications. Figure 9(a) depicts the calculated reflectivity spectra of In_2PtX_6 at photon energies up to 7 eV. For In_2PtCl_6, In_2PtBr_6, and In_2PtI_6 compounds, the reflectivity is 15%, 19%, and 25%, respectively, in the low-energy regime yielding a good performance of a transparent coating both in the visible and ultraviolet windows. Within the considered energy range, In_2PtBr_6 has a low reflectance. Additionally, the maximum peak reaches 42% for In_2PtI_6 in the high-energy region (5.69 eV).

The energy loss function is a crucial metric for determining how much energy is lost when electrons traverse through a material. The energy loss function is based on the real and imaginary parts of the dielectric function, and the peaks correspond to the typical plasma oscillation. Based on $\varepsilon_1(\omega)$ and $\varepsilon_2(\omega)$, the energy loss function can be evaluated as follows $L(\omega) = \varepsilon_2(\omega)/[\varepsilon_1^2(\omega) + \varepsilon_2^2(\omega)]$. The plots of energy loss function versus photon energy are displayed in Figure 9(b). Apparently, the energy loss is minimal when the photon energy is less than 2 eV. Figure 9(b) shows two regions where the energy loss is very large. For In_2PtI_6, the two peak energy losses are related to photon energies of 2.69 eV and 6.73 eV, respectively. For In_2PtBr_6, both peak energy losses occur at photon energies of 2.91 eV and 6.23 eV, respectively. For In_2PtCl_6, the energy losses are found at 3.46 eV and in the higher energy range (>7 eV), which is situated within the ultraviolet spectral range.

The calculated refractive index n(ω) and extinction coefficient k(ω) versus photon energy are illustrated in Figures 9(c,d). The refractive index measures how fast light travels across a material, while the extinction coefficient describes how much of the beam is lost as it goes through the medium. Such a loss is caused by the absorption and scattering per unit distance of the material. The static refractive index n(0) are acquired to be 3.02, 2.57, and 2.31 respectively for In_2PtI_6, In_2PtBr_6, and In_2PtCl_6. Increasing beyond the zero-frequency limit, it reaches a maximum value of 3.59 at ~3.93 eV (In_2PtI_6). It starts decreasing consistently with photon energy after reaching its maximum. The noticeable drop in refractive index is more likely caused by the optical dispersion behaviour of the material. On the other hand, the extinction coefficient, k(ω), has a profile that resembles the absorption coefficient α(ω) and the imaginary part of the dielectric constant (Figure 9d). It is seen that k(ω) reveals significant absorption with the peaks situated at ~2.14 and 5.51 eV for In_2PtI_6, whereas the peak values are located at ~5.07 and ~5.35 eV, respectively, for In_2PtBr_6 and In_2PtCl_6.

Photovoltaic performance of a material is determined by the spectroscopic-limited-maximum-efficiency (See Supplementary Information for detail). In a number of ways, the SLME metric outperforms the Shockley–Queisser limit, including the band gap (magnitude and nature), absorption coefficient, and suitable material thickness.[46] It also approximates the non-radiative recombination rate, which is the difference between the fundamental band gap and the direct permitted band gap. The SLME for the selected compounds was calculated under the above screening criteria (Figure 10). For comparison purposes, the SLME value of $MAPbI_3$ is also presented in Figure 10. Our calculations demonstrate that all the compounds have a maximum theoretical efficiency comparable to the champion perovskite ($MAPbI_3$) and can be used as

suitable replacements for Pb-based halide perovskites. The efficiency increases sharply with film thickness and is found maximum for In_2PtI_6 (~25%), possibly due to their proper band gap being closer to the ideal limit (1.34 eV).

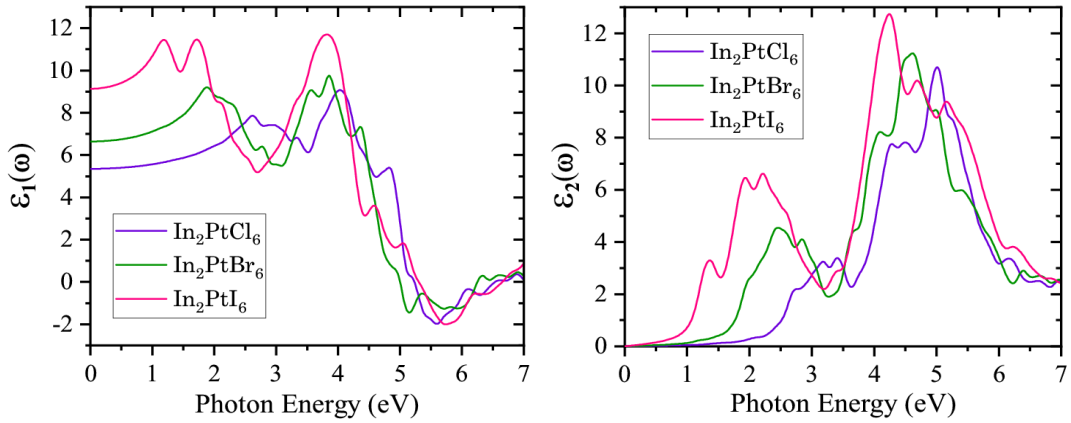

Figure 7. The frequency-dependent real (left panel) and imaginary dielectric constant (right panel) for In_2PtCl_6, In_2PtBr_6, and In_2PtI_6 versus photon energy.

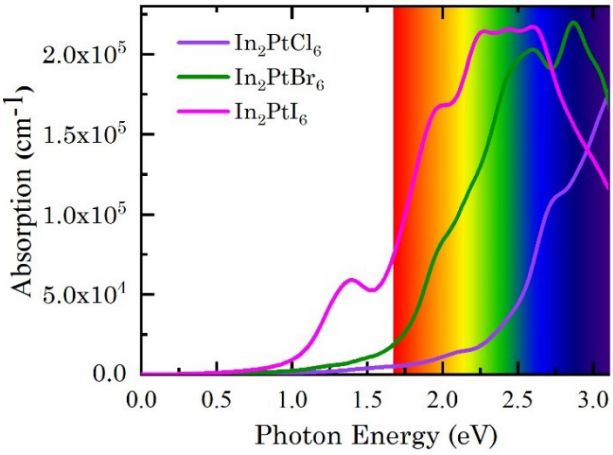

Figure 8. The absorption spectra of In_2PtCl_6, In_2PtBr_6, and In_2PtI_6 versus photon energy.

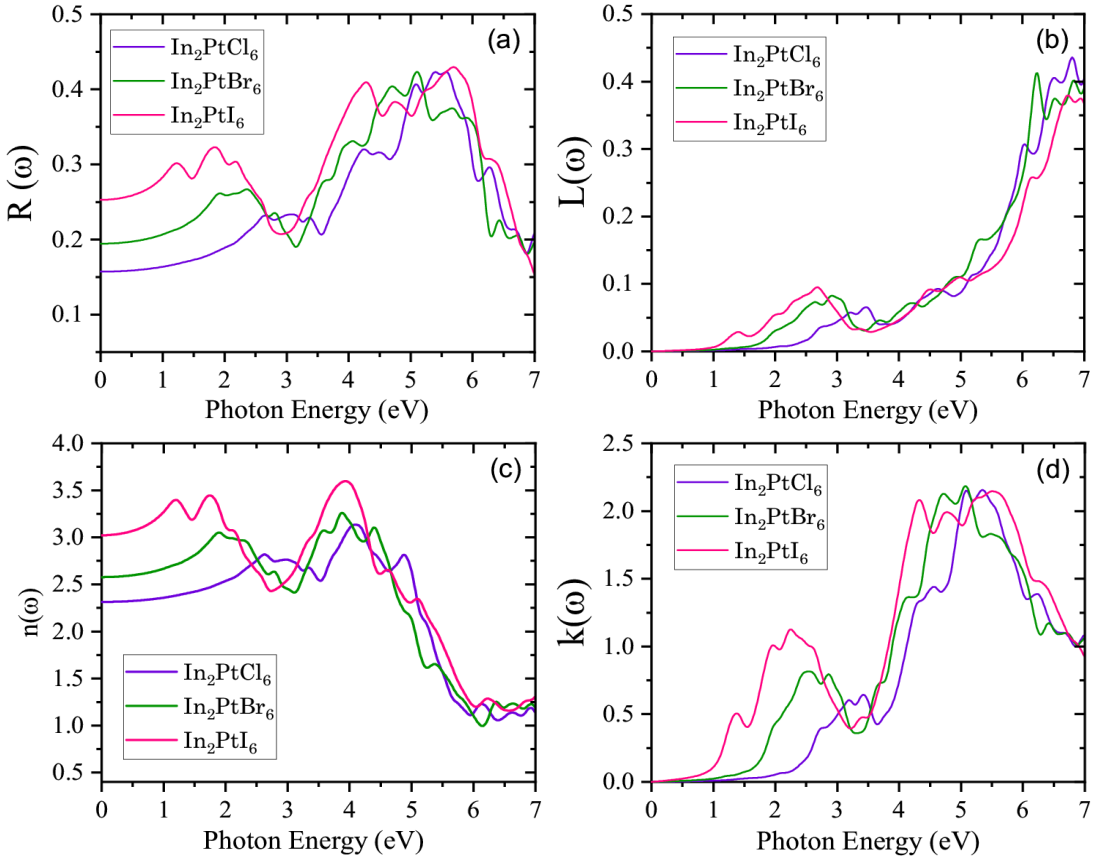

Figure 9. The calculated reflectivity coefficient R(ω) (a), the energy loss function L(ω) (b), refractive index n(ω) (c), and extinction coefficient k(ω) (d) of In_2PtX_6 (X= Cl, Br, I).

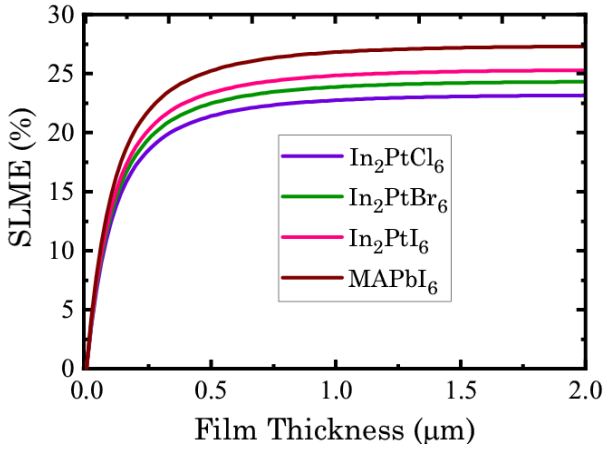

Figure 10. Calculated maximum theoretical efficiencies of In_2PtX_6 compared to lead-based perovskite absorber.

4. Conclusions

We have examined the Pb-free inorganic perovskite In_2PtX_6 with (X= halogens) for potential photovoltaic applications. A DFT-based computational technique has been employed throughout to explain and guide experiments for novel energy materials in the perovskite

family. Our study focuses primarily on the thermodynamic stability, electronic band gap, static and maximum dielectric constants, absorption spectra, and effective masses of the systems under research by using PBE and mBJ functional. Based on our phonon and AIMD simulation, In_2PtX_6 perovskites show dynamical and thermal stability. Unfortunately, the energies above hull are positive and indicates the series are unstable. By altering the halide ion from Cl to Br and then to I, the structural examination revealed that the lattice constant and volume increase monotonously, which results in an increase in Pt-X bond length. Alternatively, the band gaps and effective masses illustrate a decreasing trend when the halogens ion is varied in the same fashion. The electronic properties show ideal band gap values with direct/indirect transition nature. The In_2PtI_6 perovskite has a favourable band gap of 1.35 eV and SLME of ~25% for single-junction photovoltaic cells. It was noted that the valence band maximum is dominated by Cl/Br/I-*p* orbitals, whereas the conduction band has major contribution from Pt-*d* orbitals. Additionally, In_2PtBr_6 and In_2PtI_6 exhibited maximum absorption in the visible regime, whereas the compounds displayed redshift behaviour in the absorption spectra. Overall, our work demonstrates a great promise of using halide perovskites In_2PtX_6 in energy science and optoelectronics.

Supporting Information. Optical calculation and solar cell efficiency detail, convex hull stability, mBJ-SOC band structure, band convergence and degeneracy in In_2PtBr_6 and In_2PtI_6 perovskite with PBE functional, static dielectric constant.

Acknowledgments

The authors express their gratitude to Princess Nourah bint Abdulrahman University Researchers Supporting Project (Grant No. PNURSP2022R61), Princess Nourah bint Abdulrahman University, Riyadh, Saudi Arabia. SS would like to thank Gdańsk University of Technology for the Nobelium (No. 16/2021/IDUB/I.1) grant under "The Excellence Initiative - Research University" (IDUB) programme, which is gratefully acknowledged.

References

1. Park, N.-G., Perovskite solar cells: an emerging photovoltaic technology. *Mater. Today* **2015,** *18* (2), 65-72.
2. Song, Z.; Abate, A.; Watthage, S. C.; Liyanage, G. K.; Phillips, A. B.; Steiner, U.; Graetzel, M.; Heben, M. J., Perovskite Solar Cell Stability in Humid Air: Partially

Reversible Phase Transitions in the PbI_2-CH_3NH_3I-H_2O System. *Adv. Energy Mater.* **2016,** *6* (19), 1600846.
3. Kim, H. S.; Lee, C. R.; Im, J. H.; Lee, K. B.; Moehl, T.; Marchioro, A.; Moon, S. J.; Humphry Baker, R.; Yum, J. H.; Moser, J. E., Lead iodide perovskite sensitized all-solid-state submicron thin film mesoscopic solar cell with efficiency exceeding 9%. *Sci. Rep.* **2012,** *2*, 591(1-7).
4. Lee, B.; He, J.; Chang, R. P.; Kanatzidis, M. G., All-solid-state dye-sensitized solar cells with high efficiency. *Nature* **2012,** *485* (7399), 486-489.
5. Baikie, T.; Fang, Y.; Kadro, J. M.; Schreyer, M.; Wei, F.; Mhaisalkar, S. G.; Graetzel, M.; White, T. J., Synthesis and crystal chemistry of the hybrid perovskite $(CH_3NH_3)PbI_3$ for solid-state sensitised solar cell applications. *J. Mater. Chem. A* **2013,** *1* (18), 5628-5641.
6. Zhou, H.; Chen, Q.; Li, G.; Luo, S.; Song, T.-b.; Duan, H.-S.; Hong, Z.; You, J.; Liu, Y.; Yang, Y., Interface engineering of highly efficient perovskite solar cells. *Science* **2014,** *345* (6196), 542-546.
7. Giorgi, G.; Fujisawa, J.-I.; Segawa, H.; Yamashita, K., Small photocarrier effective masses featuring ambipolar transport in methylammonium lead iodide perovskite: a density functional analysis. *J. Phys. Chem. Lett.* **2013,** *4* (24), 4213-4216.
8. Frohna, K.; Deshpande, T.; Harter, J.; Peng, W.; Barker, B. A.; Neaton, J. B.; Louie, S. G.; Bakr, O. M.; Hsieh, D.; Bernardi, M., Inversion symmetry and bulk Rashba effect in methylammonium lead iodide perovskite single crystals. *Nat. Commun.* **2018,** *9* (1), 1829(1-9).
9. Stranks, S. D.; Eperon, G. E.; Grancini, G.; Menelaou, C.; Alcocer, M. J.; Leijtens, T.; Herz, L. M.; Petrozza, A.; Snaith, H. J., Electron-hole diffusion lengths exceeding 1 micrometer in an organometal trihalide perovskite absorber. *Science* **2013,** *342* (6156), 341-344.
10. Kojima, A.; Teshima, K.; Shirai, Y.; Miyasaka, T., Organometal halide perovskites as visible-light sensitizers for photovoltaic cells. *J. Am. Chem. Soc.* **2009,** *131* (17), 6050-6051.
11. NREL, Best Research-Cell Efficiencies https://www.nrel.gov/pv/assets/pdfs/best-research-cell-efficiencies-rev220126.pdf (NREL, accessed 2022-01-16).
12. Umari, P.; Mosconi, E.; De Angelis, F., Relativistic GW calculations on $CH_3NH_3PbI_3$ and $CH_3NH_3SnI_3$ perovskites for solar cell applications. *Sci. Rep.* **2014,** *4* (1), 1-7.
13. Bass, K. K.; McAnally, R. E.; Zhou, S.; Djurovich, P. I.; Thompson, M. E.; Melot, B. C., Influence of moisture on the preparation, crystal structure, and photophysical properties of organohalide perovskites. *ChemComm.* **2014,** *50* (99), 15819-15822.
14. Mosconi, E.; Azpiroz, J. M.; De Angelis, F., Ab initio molecular dynamics simulations of methylammonium lead iodide perovskite degradation by water. *Chem. Mater.* **2015,** *27* (13), 4885-4892.
15. Hailegnaw, B.; Kirmayer, S.; Edri, E.; Hodes, G.; Cahen, D., Rain on methylammonium lead iodide based perovskites: possible environmental effects of perovskite solar cells. *J. Phys. Chem. Lett.* **2015,** *6* (9), 1543-1547.
16. Yang, B.; Li, Y.-J.; Tang, Y.-X.; Mao, X.; Luo, C.; Wang, M.-S.; Deng, W.-Q.; Han, K.-L., Constructing sensitive and fast lead-free single-crystalline perovskite photodetectors. *J. Phys. Chem. Lett.* **2018,** *9* (11), 3087-3092.
17. Jodlowski, A.; Rodríguez-Padrón, D.; Luque, R.; de Miguel, G., Alternative Perovskites for Photovoltaics. *Adv. Energy Mater.* **2018,** *8* (21), 1703120.
18. Lee, B.; Stoumpos, C. C.; Zhou, N.; Hao, F.; Malliakas, C.; Yeh, C.-Y.; Marks, T. J.; Kanatzidis, M. G.; Chang, R. P., Air-stable molecular semiconducting iodosalts for

solar cell applications: Cs_2SnI_6 as a hole conductor. *J. Amer. Chem. Soc.* **2014,** *136* (43), 15379-15385.
19. Ju, M.-G.; Chen, M.; Zhou, Y.; Garces, H. F.; Dai, J.; Ma, L.; Padture, N. P.; Zeng, X. C., Earth-abundant nontoxic titanium (IV)-based vacancy-ordered double perovskite halides with tunable 1.0 to 1.8 eV bandgaps for photovoltaic applications. *ACS Energy Lett.* **2018,** *3* (2), 297-304.
20. Tan, Z.; Li, J.; Zhang, C.; Li, Z.; Hu, Q.; Xiao, Z.; Kamiya, T.; Hosono, H.; Niu, G.; Lifshitz, E., Highly Efficient Blue-Emitting Bi-Doped Cs_2SnCl_6 Perovskite Variant: Photoluminescence Induced by Impurity Doping. *Adv. Funct. Mater.* **2018,** *28* (29), 1801131.
21. Schwartz, D.; Murshed, R.; Larson, H.; Usprung, B.; Soltanmohamad, S.; Pandey, R.; Barnard, E. S.; Rockett, A.; Hartmann, T.; Castelli, I. E., Air Stable, High-Efficiency, Pt-Based Halide Perovskite Solar Cells with Long Carrier Lifetimes. *Phys. Status Solidi - Rapid Res. Lett.* **2020,** *14* (8), 2000182.
22. Faizan, M.; Khan, S. H.; Khachai, H.; Seddik, T.; Omran, S. B.; Khenata, R.; Xie, J.; AL-Anazy, M. m., Electronic, optical, and thermoelectric properties of perovskite variants A_2BX_6: Insight and design via first-principles calculations. *Int. J. Energy Res.* **2021,** *45* (3), 4495-4507.
23. Faizan, M.; Xie, J.; Murtaza, G.; Echeverría-Arrondo, C.; Alshahrani, T.; Bhamu, K. C.; Laref, A.; Mora-Seró, I.; Khan, S. H., A first-principles study of the stability, electronic structure, and optical properties of halide double perovskite $Rb_2Sn_{1-x}Te_xI_6$ for solar cell applications. *Phys. Chem. Chem. Phys.* **2021,** *23* (8), 4646-4657.
24. Kaltzoglou, A.; Antoniadou, M.; Kontos, A. G.; Stoumpos, C. C.; Perganti, D.; Siranidi, E.; Raptis, V.; Trohidou, K.; Psycharis, V.; Kanatzidis, M. G., Optical-vibrational properties of the Cs_2SnX_6 (X= Cl, Br, I) defect perovskites and hole-transport efficiency in dye-sensitized solar cells. *J. Phys. Chem. C* **2016,** *120* (22), 11777-11785.
25. Zhao, X.-H.; Wei, X.-N.; Tang, T.-Y.; Gao, L.-K.; Xie, Q.; Lu, L.-M.; Tang, Y.-L., First-principles study on the structural, electronic and optical properties of vacancy-ordered double perovskites Cs_2PtI_6 and Rb_2PtI_6. *Opt. Mater.* **2021,** *114*, 110952.
26. Sajjad, M.; Mahmood, Q.; Singh, N.; Larsson, J. A., Ultralow Lattice Thermal Conductivity in Double Perovskite Cs_2PtI_6: A Promising Thermoelectric Material. *ACS Appl. Energy Mater.* **2020,** *3* (11), 11293-11299.
27. Alhodaib, A., Study of vacancy ordered double perovskites In_2PtX_6 (X= Cl, Br, I) for solar cells and renewable energy, alternative of hybrid perovskites. *J. Solid State Chem.* **2022,** *309*, 123015.
28. Blaha, P.; Schwarz, K.; Tran, F.; Laskowski, R.; Madsen, G. K.; Marks, L. D., WIEN2k: An APW+ lo program for calculating the properties of solids. *J. Chem. Phys.* **2020,** *152* (7), 074101.
29. Al, S.; Arikan, N.; Iyigör, A., Investigations of structural, elastic, electronic and thermodynamic properties of X_2TiAl Alloys: a computational study. *Z. Naturforsch. A* **2018,** *73* (9), 859-867.
30. Perdew, J. P.; Burke, K.; Ernzerhof, M., Generalized gradient approximation made simple. *Phys. Rev. Lett.* **1996,** *77* (18), 3865.
31. Tran, F.; Blaha, P., Accurate band gaps of semiconductors and insulators with a semilocal exchange-correlation potential. *Phys. Rev. Lett.* **2009,** *102* (22), 226401.
32. Heyd, J.; Scuseria, G. E.; Ernzerhof, M., Hybrid functionals based on a screened Coulomb potential. *J. Chem. Phys.* **2003,** *118* (18), 8207-8215.
33. Maughan, A. E.; Ganose, A. M.; Bordelon, M. M.; Miller, E. M.; Scanlon, D. O.; Neilson, J. R., Defect tolerance to intolerance in the vacancy-ordered double perovskite semiconductors Cs_2SnI_6 and Cs_2TeI_6. *J. Am. Chem. Soc.* **2016,** *138* (27), 8453-8464.

34. Jong, U.-G.; Kim, Y.-S.; Ri, C.-H.; Kye, Y.-H.; Pak, C.-J.; Cottenier, S.; Yu, C.-J., Twofold rattling mode-induced ultralow thermal conductivity in vacancy-ordered double perovskite Cs_2SnI_6. *ChemComm.* **2022,** *58* (26), 4223-4226.
35. Nosé, S., A unified formulation of the constant temperature molecular dynamics methods. *Chem. Phys.* **1984,** *81* (1), 511-519.
36. Sakai, N.; Haghighirad, A. A.; Filip, M. R.; Nayak, P. K.; Nayak, S.; Ramadan, A.; Wang, Z.; Giustino, F.; Snaith, H. J., Solution-processed cesium hexabromopalladate (IV), Cs_2PdBr_6, for optoelectronic applications. *J. Am. Chem. Soc.* **2017,** *139* (17), 6030-6033.
37. Mosconi, E.; Amat, A.; Nazeeruddin, M. K.; Grätzel, M.; De Angelis, F., First-principles modeling of mixed halide organometal perovskites for photovoltaic applications. *J. Phys. Chem. C* **2013,** *117* (27), 13902-13913.
38. Shockley, W.; Queisser, H. J., Detailed balance limit of efficiency of p-n junction solar cells. *J. Appl. Phys.* **1961,** *32* (3), 510-519.
39. Kang, E. S.; Ismail, R., Analytical performance of 3 m and 3 m+ 1 armchair graphene nanoribbons under uniaxial strain. *Nanoscale Res. Lett.* **2014,** *9* (1), 1-8.
40. Cai, Y.; Xie, W.; Ding, H.; Chen, Y.; Thirumal, K.; Wong, L. H.; Mathews, N.; Mhaisalkar, S. G.; Sherburne, M.; Asta, M., Computational Study of Halide Perovskite-Derived A_2BX_6 Inorganic Compounds: Chemical Trends in Electronic Structure and Structural Stability. *Chem. Mater.* **2017,** *29* (18), 7740-7749.
41. Faizan, M.; Bhamu, K.; Murtaza, G.; He, X.; Kulhari, N.; AL-Anazy, M. M.; Khan, S. H., Electronic and optical properties of vacancy ordered double perovskites A_2BX_6 (A= Rb, Cs; B= Sn, Pd, Pt; and X= Cl, Br, I): a first principles study. *Sci. Rep.* **2021,** *11* (1), 1-9.
42. Feng, J.; Xiao, B., Effective masses and electronic and optical properties of nontoxic $MASnX_3$ (X= Cl, Br, and I) perovskite structures as solar cell absorber: a theoretical study using HSE06. *J. Phys. Chem. C* **2014,** *118* (34), 19655-19660.
43. Zhao, X.-G.; Yang, D.; Sun, Y.; Li, T.; Zhang, L.; Yu, L.; Zunger, A., Cu–In halide perovskite solar absorbers. *J. Am. Chem. Soc.* **2017,** *139* (19), 6718-6725.
44. Meng, W.; Saparov, B.; Hong, F.; Wang, J.; Mitzi, D. B.; Yan, Y., Alloying and defect control within chalcogenide perovskites for optimized photovoltaic application. *Chem. Mater.* **2016,** *28* (3), 821-829.
45. Meng, W.; Wang, X.; Yan, Y.; Wang, J., Stability, Electronic and Optical Properties of $M_4M'X_4$ (M= Ga or In, M′= Si, Ge, or Sn, X= Chalcogen) Photovoltaic Absorbers. *J. Phys. Chem. C* **2018,** *122* (19), 10360-10364.
46. Yu, L.; Zunger, A., Identification of potential photovoltaic absorbers based on first-principles spectroscopic screening of materials. *Phys. Rev. Lett.* **2012,** *108* (6), 068701.

TOC Entry